ORIGINAL PAPER: NANO- AND MACROPOROUS MATERIALS (AEROGELS, XEROGELS, CRYOGELS, ETC.)



How addition of a nickel cyclohexyl-salen complex impacts a one-pot synthesis of nickel/hierarchically porous carbon monolith catalyst

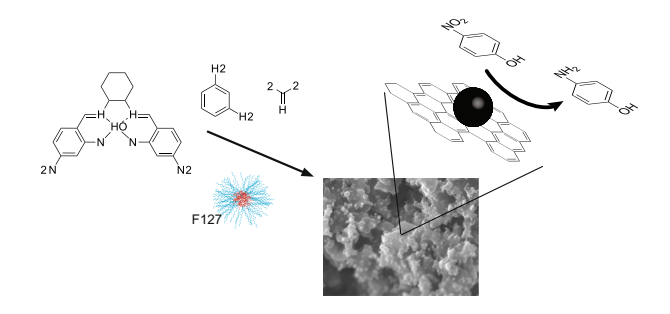
Rina Adhikari¹ · Trupti V. Kotbagi¹ · Kevin H. Shaughnessy¹ · Ambar B. Shrestha¹ · Jennifer Sherwood² · Yuping Bao² · Martin G. Bakker 60¹

Received: 3 September 2020 / Accepted: 27 October 2020 / Published online: 14 November 2020 © Springer Science+Business Media, LLC, part of Springer Nature 2020

Abstract

Synthesis of hierarchically porous carbons incorporating metal nanoparticles can be carried out by a "one-pot" process in which the metal precursor is mixed with polymer precursors and structure directing agents, that undergoes a sol-gel self-assembly polymerization and then pyrolyzed under an inert atmosphere. Such syntheses are potentially cheaper and could make carbon catalysts more compatible with organic solvents. Previous work had shown that addition of metal salts interfered with the self-assembly process. To prevent this interference, and increase thermal stability, a nickel cyclohexyl salen complex was used as metal precursor. Dynamic light scattering (DLS) of the precursor solutions shows the presence of micelles in the absence of added complex. Addition of the complex is observed to give large agglomerates and a reduction in micelle concentration. SEM of the carbons formed shows that the nickel particles have a wide distribution of particle sizes and a heterogenous spatial distribution. Gas adsorption showed only modest changes resulting from nickel complex addition. XRD confirms the formation of nickel nanoparticles. The heterogenous distribution of nanoparticles observed in SEM is consistent with the large agglomerates observed in DLS being nickel cyclohexyl-salen complex which is not fully dispersed in the polymer and therefore gives heterogenous dispersion in the resulting carbon. The metal dispersion and stability of the carbon were improved over that observed with other salen complexes. The resulting catalysts were found to be catalytically active for the reduction of *p*-nitrophenol by sodium borohydride with catalytic activity consistent with the particle size distributions.

Graphical Abstract



Supplementary information The online version of this article (https://doi.org/10.1007/s10971-020-05436-3) contains supplementary material, which is available to authorized users.

- Martin G. Bakker bakker@ua.edu
- Department of Chemistry and Biochemistry, The University of Alabama, Box 870336, Tuscaloosa, AL 35487-0336, USA
- Department of Chemical and Biochemical Engineering, The University of Alabama, Box 870203, Tuscaloosa, AL 35487-0203, USA



Keywords Porous Carbon · Nickel · One-pot synthesis · Reduction · p-nitrophenol

Highlights

- Nickel nanoparticles on hierarchically macro-mesoporous carbon monolith.
- Polymerization of organic monomers + nickel complex + structure directing agents.
- Limited solubility of nickel complex interferes with self-assembly.
- Nickel complex structure found to impact carbon stability.
- Monolithic catalyst is catalytically active for hydrogenation.

1 Introduction

Many large-scale industrial processes are carried out as continuous processes using fixed bed catalysts. The use of a supported catalyst eliminates the need for a process to separate the catalyst from the reaction products thereby reducing cost, both in capital expense and in terms of energy usage. Carbon is one of the most widely used supports for fixed-bed catalysts, with carbon produced from many natural sources such as peat, wood, walnut shells, and coconut husks being used commercially [1, 2]. These naturally sourced carbons bring advantages such as low cost and high surface area over which catalytic metal nanoparticles are dispersed, however, diffusion of reactants into the bulk of the catalyst particles is often limited, reducing the active volume [3]. Developing a fully synthetic alternative in which the porosity could be controlled at multiple length scales has been of interest not just for fixed-bed catalysis applications, but also for adsorbents, supercapacitors and electrochemical applications. Early work in the polymerization of resorcinol-formaldehyde aerogels gave high surface area materials [4, 5] in a synthesis that was shown to be compatible with the incorporation of metal salts [6–8]. However, aerogels tend to be mechanically fragile, which makes them unsuitable for fixed bed reactors. Some progress has been made in overcoming this problem [9–11], but the highest reported compression strength is still only 5 MPa, which is short of what is typical for fixed bed reactor applications. A more promising path forward is based on the use of surfactant templating to create ordered mesopores coupled with polymerization induced phaseseparation to produce controlled macroporosity [12-22]. These materials are reported to have compression strength of up to 15.6 MPa, which is high enough for fixed bed reactors. They are attractive materials for this application, as the interconnecting network of macropores within these materials should give better mass transport into a catalytic particle and so higher catalytic efficiency. In the limit, a single piece of porous carbon can function as a monolithic reactor in a fashion analogous to what is seen in automotive catalytic convertors [23, 24]. For automotive applications the monoliths typically have macropore diameters of 0.5–1 mm. In contrast, for hierarchically porous monoliths incorporating macropores and mesopores, typical macropore dimensions are in the 10-30-um range, potentially giving much higher accessible surface area. A handful of groups have begun to explore the potential of these materials for fixed-bed catalysis as a monolithic microreactor [25–31], but all these examples used silica columns, which were developed in the early 1990's. The development of hierarchically porous carbon monolith synthesis is much more recent, and the advantages and disadvantages of carbon supports are different from those of silica. Carbon is more chemically stable than silica, particularly under hydrothermal conditions, and has better electrical and thermal conductivity, but is less readily functionalized than silica. Syntheses based on carbon-based monomers are potentially capable of a much wider range of polymerization reactions and synthetic complexity, being able to tap into the large reservoir of organic compounds and methods already developed.

We have begun exploring the potential of modifying the polymerization reactions to tackle one of the shortcomings of many commercial carbon supports, which is the need to activate the carbon surface to provide the surface functionality needed to give good dispersion of metal nanoparticles in fixed bed catalysts. By including metal salts with the polymer precursors in a resorcinol/ formaldehyde polymerization it has been possible to produce hierarchically porous carbon monoliths that contain palladium [32] and nickel nanoparticles [33, 34]. Such syntheses are potentially cheaper as well as producing catalysts that are less hydrophilic than tradition activated catalysts. However, it was observed that with increasing metal salt concentration, the volume of mesopores decreased [33, 34]. This was ascribed to binding of the metal ions to diaminohexane, one of the structure-directing agents. In order to overcome this, we proposed and tested the use of salen ligands to bind up the transition metal ions and so prevent them interfering with the self-assembly process [35]. The salen ligands used are structurally similar to the resorcinol used in the polymerization and so could co-polymerize to give better dispersion of the metal salt within the polymer. The two salen ligands used are



Scheme 1 Structure of ligands

shown in Scheme 1 and contain a two-carbon bridge between two halves of the ligand (E-salen) and a sixcarbon bridge (D-salen). A large difference in metal nanoparticle dispersion was found between the E-salen and D-salen ligands, with the E-salen ligand giving smaller nanoparticles for all three metals studied, and the D-salen giving rise to nanowires and well formed, large metal crystals. It was suggested that the difference in result reflected the weaker binding of the metal ions to the Dsalen ligand due to the formation of a thermodynamically unfavorable eight membered ring [35]. Converting this eight-membered ring into a more thermodynamically favorable cyclohexyl ring, would also impart more rigidity into the complex, and so it is predicted that a better dispersion of metal nanoparticles should result. This contribution tests this prediction by synthesizing the C-salen ligand, and binding nickel ions to give the nickel C-salen complex and adding this complex into the polymer precursors. It also explores the details of the polymerization/ self-assembly process using dynamic light scattering and assesses the catalytic activity of the resulting nickel supported on hierarchically porous carbon catalyst.

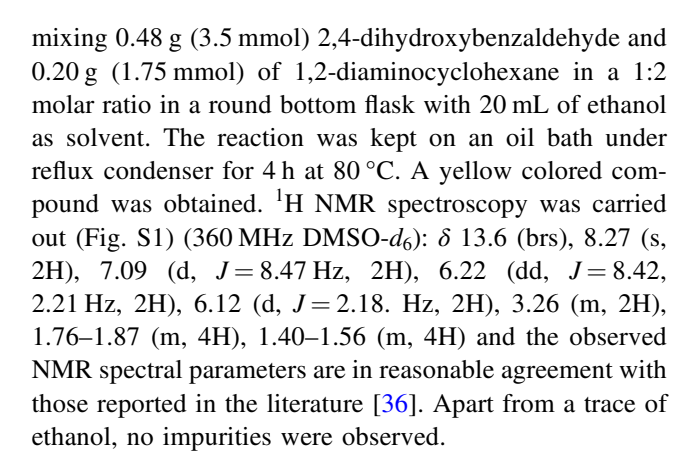
2 Experimental

2.1 Chemicals

Formaldehyde as formalin, a 36.5–38% solution in water, Macron® brand, was obtained from Avantor, Pluronic F127 (HO–(CH₂ -CH₂O)₁₀₀ –(CH₂ -CH(CH₃)O)₆₅ –(CH₂CH₂O)₁₀₀–OH: PEO₁₀₀-PPO₆₅-PEO₁₀₀) from Spectrum Chemicals, 1,6-hexanediamine (DAH) from Acros Organics, 99%, resorcinol (1,3-dihydroxybenzene), 98%, 2,4-dihydroxybenzaldehyde and 99% 1,2-diaminocyclohexane (mixture of cis- and trans- isomers) from Sigma Aldrich, 99%, nickel acetate tetrahydrate and 97% cobalt acetate tetrahydrate from Acros Organics, 100% dimethyl sulfoxide (DMSO) CalbiochemTM, 98% furfural from Alfa Aesar and *p*-nitrophenol (PNP) was obtained from VWR. Unless specified otherwise, all chemicals were used as obtained without further purification.

2.2 Preparation of C-salen ligand

The C-salen ligand (4,4'-[1,2-cyclohexanediylbis(nitrilomethylidyne)]bis-1,3-benzenediol) was prepared by



2.3 Preparation of Nickel-C-salen complex

For synthesis of the nickel-C-salen complexes 0.28 g of C-salen ligand and 0.40 g of nickel acetate tetrahydrate were mixed in a 1:1 molar ratio in a 30 mL round bottom flask with 20 mL ethanol as solvent. The reaction mixture was kept in an oil bath with condenser at 80 °C for 6 h. The orange-colored compound precipitated from the solution and was then separated by filtration. Ni-C-Salen would be expected to be nonparamagnetic and ¹H NMR spectroscopy was carried out (Fig. S2) (360 MHz, DMSO-*d*):δ 9.75 (brs, 2 H), 7.51 (brs, 2 H), 7.15 (s, 2 H), 6.03 (s, 4H), 2.95 (2 H), 2.42 (2H) 1.72 (2H), 1.21 (4H), which is consistent with the expected spectrum from Ni-C-salen.

2.4 Synthesis of direct carbon-metal complex impregnated carbon monoliths

For a typical synthesis of carbon monoliths 4.54 g of resorcinol and 1.8 g of F127 were dissolved in 13.5 g of EtOH and 13.5 g of H₂O in a 250 mL beaker. The solution was stirred until the solids completely dissolved (with a measured pH = 6.22). To this solution, 0.117 g of DAH was added and stirred (pH = 8.092). If metal was incorporated, then the metal salen was first dissolved in a small (ca. 2 mL) amount of DMSO and added to the reaction mixture. The addition of Ni-C-salen gave the solution a deep orange color. Initially some undissolved lumps were observed but with stirring the color spread uniformly. Finally, 6 g of formalin was added with stirring. Within a few minutes the solution was observed to turn cloudy and became viscous (pH = 7.53). The solution was then transferred to 10 mL centrifuge tubes, which were sealed and placed in a pressure cooker containing 30 mL of water and 30 mL of ethanol and allowed to cure for 6 h at 80 °C. The curing was followed by drying for 12 h at 60 °C.

After drying, the samples were reddish brown in color and sufficiently stiff that they could be removed from the centrifuge tubes and cut into small pieces of circular shape



and ~10 mm in length. For metal complex impregnated samples the dried polymer was a deep orange color that extended all the way through the sample. Sections were carbonized under a nitrogen atmosphere at 500 and 800 °C, at ramp rates of 1.33, and 2.16 degrees per minute, respectively, with the final temperature held for 2 h. These samples will be referred to as DC-X where X = the pyrolysis temperature. The nickel containing sample will be referred to as YNiCsalCX, where Y is the wt% nickel and X is the temperature. The amount of the C-salen complex added was calculated by assuming that no nickel was lost during the polymerization. The mass of carbon and nitrogen produced by pyrolysis to 500 °C, i.e., the yield of carbon, was determined by a separate experiment (detail given in supplementary information) to be 49.4% based on the amount of resorcinol used in the synthesis. The samples pyrolyzed to 800 °C used the same complex to resorcinol ratio as the samples for 500 °C. In going from pyrolysis at 500 °C to pyrolysis at 800 °C there is a further loss of mass [35], and so 1 wt%NiCsalC800 is actually 1.13% nickel by weight, and the 5 wt%NiCsalC800 sample is 5.65% by weight nickel.

2.5 Catalysis

To test the catalytic activity, 20 mg of ground catalyst was used in 50 mL of 100 μ M PNP to which was added 25 mL of 0.4 M NaBH₄ as reducing agent. The reaction was done in a flask with magnetic stirring. A 3 mL aliquot was drawn every minute and a UV/vis scan was done with a Shimadzu UV/Vis spectrometer. The concentration of the reactant was determined from the absorbance maxima.

2.6 Characterization

The SEM images were taken on a JEOL 7000 FE-SEM (Tokyo, Japan) using a positive bias on an Everhart Thornley (E-T) detector for secondary electron imaging (SEI), a solid-state diode backscatter detector for composition (COMPO) and an Oxford Energy Dispersive Spectroscopy (EDS) detector for elemental analysis. The cylindrical samples were cut perpendicular to the long axis of the cylinder to give circular cross-sections with a razor blade and mounted such that the cross-section was imaged. This procedure removed any potential artifacts that might result from imaging interfaces (either air/solution, or plastic/solution). Surface area was analyzed using a Quantachrome Nova 2200e pore size analyzer (Boynton Beach FL) at 77 K with He mode for void volume correction. Interpretation of the isotherms was done with Quantachrome Novawin software version 11.1 using NL-DFT to obtain surface area for carbon. The pore size distribution was determined by applying NL-DFT to the adsorption branch of the nitrogen adsorption isotherm. The XRD data were taken using a Bruker D8 Discover XRD with GADDS software.

3 Results

3.1 **SEM**

The SEM images of the various samples are shown in Figs 1-5. The macropores are seen in Fig. 1. The images of 1% nickel loaded carbon heated to 500 and 800 °C are shown in Figs 2 and 3, respectively. At the lower carbonization temperature, relatively few nanoparticles were seen, and these primarily as isolated individual particles on the macropore walls. There were also a few instances of clusters of nanoparticles as seen in Fig. 2b. EDS and backscatter (Figs S2-5) confirms that these are nickel nanoparticles. For the sample heated to 800 °C (Fig. 3), the surface of the macropores was covered with nickel nanoparticles, including several of relatively large (~50-100 nm) size. Figure 3c shows a particularly interesting location. The flat surface seen in the image is the cross-section of a ligament and shows a cluster of larger nanoparticles in the core of the ligament. For 5% Ni loaded samples (Figs 4 and 5), significantly more nanoparticles are visible on the macropore walls even when the sample was heated to only 500 °C. More particles were visible for the 800 °C sample than for the 500 °C sample. ImageJ was used to analyze the SEM image. The cross-sectional area was determined for each particle, and an average radius calculated. This was used to calculate a particle surface area assuming the particles were spheres. These are reported in Table 1. Examples of the ImageJ measurements and particle size distributions are included in the supplementary information.

EDS experiments were carried out at multiple locations in the images shown, as well as at other locations on the samples (see Supplementary information). Even areas that were devoid of nanoparticles showed the presence of a low level of nickel (typically ca. 1%). The interaction volume for the 20 keV electron beam used is of the order of 2-µm diameter for these samples and so the presence of small nickel particles within this volume cannot be completely ruled out. However, it does appear that nickel is present at some low concentration throughout the sample, with higher local concentrations.

3.2 Nitrogen Adsorption

Nitrogen adsorption isotherms of the samples, and the pore size distributions are given in Fig. 6. The surface areas and pore volumes are reported in Table 2. For the 1 wt% nickel loaded samples there is a large step at low P/Po (<0.01)



Fig. 1 SEM images of DC500 (a) lower magnification and (b) higher magnification

a Toum

Fig. 2 Images of 1% NiCsalC500 using SEI mode at (a) low magnification and (b) higher magnification

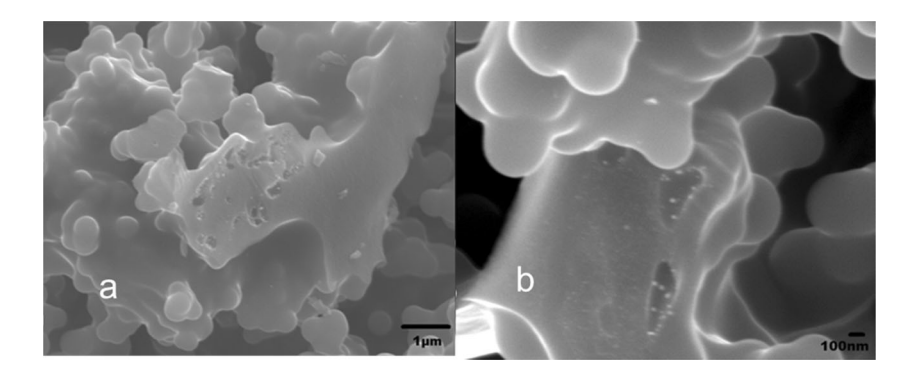
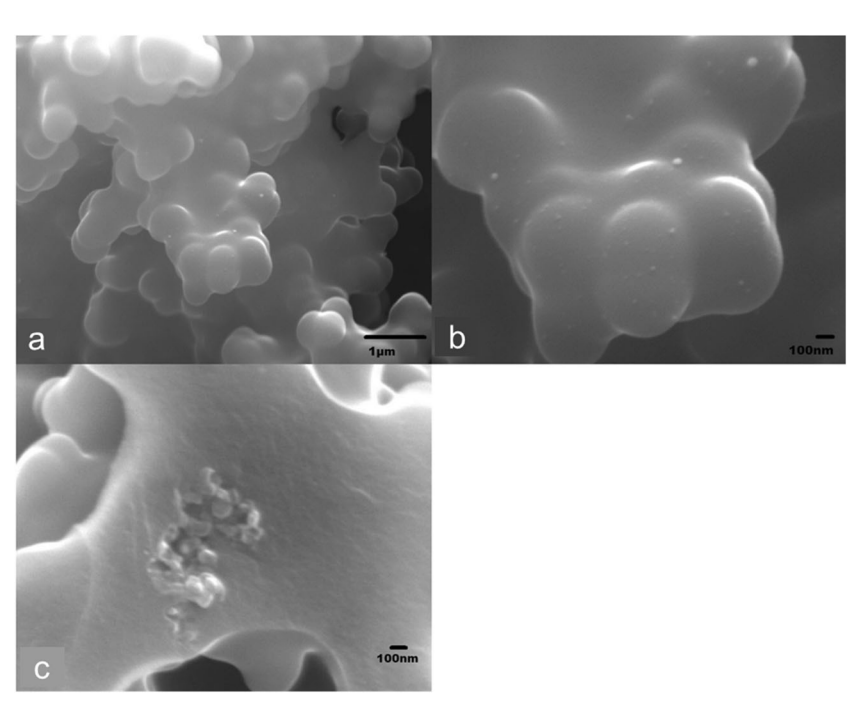


Fig. 3 SEM images of 1% NiCsalC800 using SEI mode, at (a) low magnification, (b) higher magnification (c) detail showing cross-section of ligament and cluster of nanoparticles



consistent with the presence of a significant volume of micropores in these samples. The 1 wt% nickel samples also show a significant hysteresis loop between P/Po 0.4 and 0.6 indicating a large mesopore volume. The 5 wt% nickel loaded samples have smaller hysteresis loop which could be the result of the blockage of pores by metal particles. The pore size distribution shows that each sample has a peak at

 $1.89\,\mathrm{nm}$. $5\mathrm{NiCsalC}800$ shows multiple peaks from 0.7 to $2\,\mathrm{nm}$.

3.3 XRD

The XRD diffractograms are shown in Fig. 7. There is a broad peak at around 28° that is due to amorphous carbon. For the nickel samples peaks at 42°, 46°, and 95° were



Fig. 4 SEM image of 5% NiCsalC500 using SEI mode, at (a) low magnification and (b) higher magnification

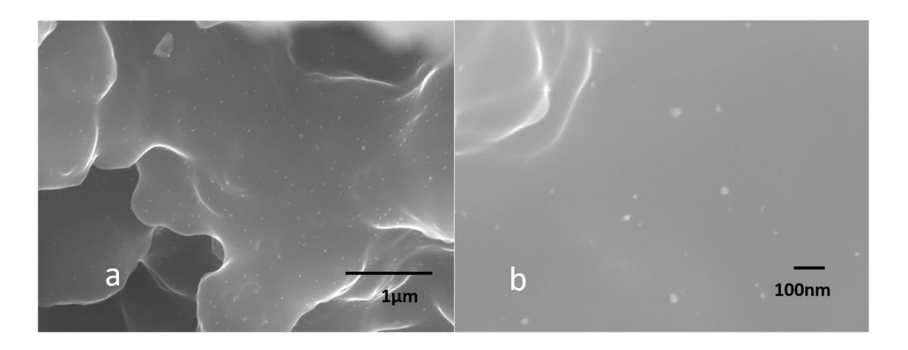


Fig. 5 SEM images of 5% NiCsalC800 using SEI mode (a) low magnification and (b) higher magnification

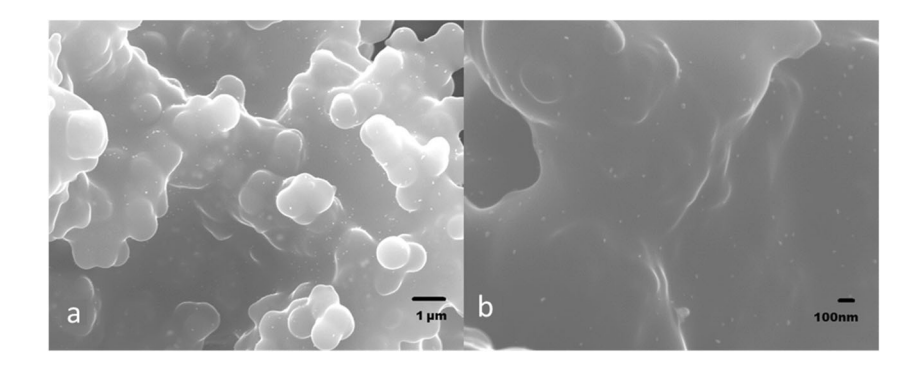


 Table 1 Nickel particle size and estimated surface area

Sample	Crystallite size from XRD (Scherrer) (nm) ^a	SEM particle size range (ImageJ) diameter (nm) ^b	Estimated nickel surface area (m²/g)
1%NiCsalC500	11	8–47 (96)	17
1%NiCsalC800	16	3–35 (151)	23
5%NiCsalC500	9	6-38 (329)	25
5%NiCsalC800	16	9–489 (143)	12

^aCalculated from Ni [200] peak

observed. The peak positions are consistent with the (111), (200), and (311) reflections for cubic phase nickel. Estimates of the average crystallite sizes of the Ni particles for the different samples were calculated from the width of the Ni (111) peaks for 1 and 5 wt% nickel loaded samples line using the Scherrer formula and are reported in Table 1.

3.4 Dynamic light scattering

DLS requires knowing the solution viscosity in order to calculate the particle size distribution from the autocorrelation function. The actual viscosities for each sample were determined using an Ostwald viscometer calibrated against water. The calculated particle size distributions and the measured viscosities are reported in the Supplementary information. The data are shown as percentage volume correcting for the lower scattering intensity of particles in the nanometer range. Table 3 shows the particle sizes

determined by DLS, corrected for changes in bulk viscosity. Detailed analysis of the experiments is given in the discussion section below.

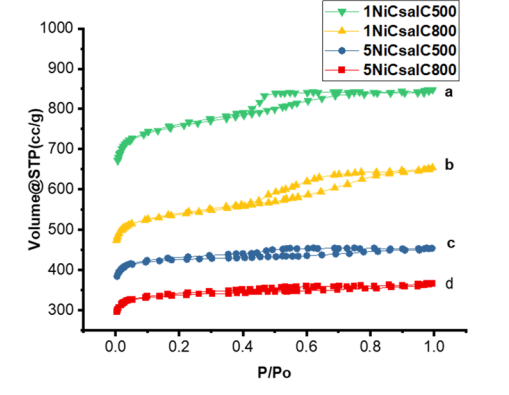
3.5 Catalysis

The catalytic activity for the reduction of p-nitrophenol (PNP) in water with sodium borohydride as the reducing agent was studied. The NaBH₄ is present in large excess (400 times [PNP]), and in each case the reaction appears to have pseudo first-order kinetics with respect to PNP. A typical UV-vis plot is shown in Fig. 8a, and the concentration variation with time is shown in Fig. 8b. Plots of Ln(Concentration) vs time give good straightline fits with R^2 values exceeding 0.99 in all cases indicating a good fit with first-order kinetics. The first-order rate constants are reported in Table 4. A blank experiment confirmed that PNP did not absorb significantly on the support.



^bNumber of particles measured in parenthesis

Fig. 6 Nitrogen physisorption isotherms of 1 and 5 wt% nickel containing carbons pyrolyzed at 500 and 800 °C. (left), (a) 1% NiCsalC500 (offset by 107 cc/g) (b) 1% NiCsalC800(offset by 140 cc/g) (c) 5% NiCsalC500 (offset by 80cc/g) and (d) 5% NiCsalC800 (offset by 0 cc/g), and pore size distribution of samples (right)



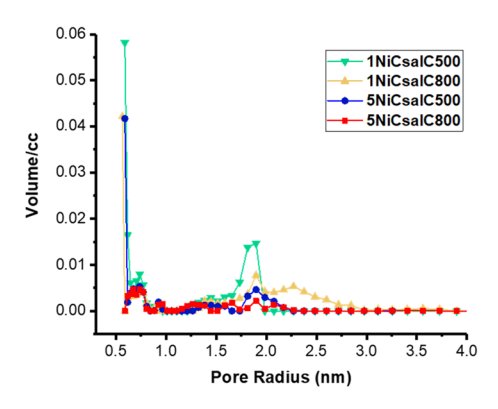


Table 2 Carbon surface area

Sample	Surface area (m²/g)	Mesopore volume (cc/g)	Micropore volume (cc/g)	Total pore volume (cc/g)	Pore radius peak (nm)
1%NiCsalC500	638	0.14	0.18	0.32	1.87
1%NiCsalC800	501	0.10	0.17	0.27	1.89
5%NiCsalC500	560	0.06	0.19	0.25	1.89
5%NiCsalC800	564	0.05	0.20	0.25	0.74, 1.89

4 Discussion

The procedure for synthesizing nickel nanoparticles supported on hierarchically porous carbon is based on a 2011 paper by Hao et al. [18]. In the supplementary information for that paper the authors report experiments that show that the role of the diaminohexane is not simply to act as a base catalyst, but that it also assists with producing the ordered mesopores.

Hao et al. [18] found that the water-insoluble polymer components are initially richer in nitrogen, and that the nitrogen concentration decreases with curing time. Recent DFT calculations [37] indicate that primary amines react with formaldehyde to give a carbinolamine:

$$CH_2 = O + HNHR \rightarrow HOCH_2 - NHR$$

Addition of a second formaldehyde gives the N,N-dihydroxymethylamine [38, 39].

$$HOCH_2NHR + CH_2 = O \rightarrow (HOCH_2)_2NR$$

This protonates with loss of water to give a reactive iminium ion [40]:

$$(HOCH_2)_2 - NR + H^+ \rightarrow H_2O + CH_2 = N^+(CH_2OH)R$$

The iminium ion is a good electrophile and reacts with resorcinol, followed by loss of water and ring closure to give a benzoxazine [38, 39]. Reactions at each end of the diaminohexane, and multiple additions to resorcinol, produce polymerization.

Based on the observations by Hao et al. it appears that this set of reactions is faster than addition of formaldehyde

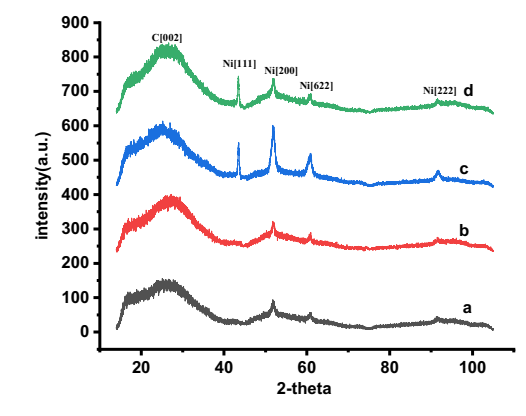


Fig. 7 XRD peaks obtained for **(a)** 1%NiCsalC500 (offset by 0), **(b)** 1%NiCsalC800 (offset by 229), **(c)** 5%NiCsalC500 (offset by 417) and **(d)** 5%NiCsalC800 (offset by 629)

directly to the resorcinol, and so formation of the gel is initially through the reaction of the DAH, and that it is primarily during curing that resorcinol/formaldehyde condensation reactions convert the soft gel into a harder polymer.

What has been unclear in this report is how the various components of the synthesis are interlinked. The DLS data begins to untangle this complexity. Experiment 1 shows that under the conditions of the synthesis procedure F127 is above the critical micelle concentration (CMC) and forms micelles. Addition of resorcinol increases the size of these micelles, and the simultaneous addition of resorcinol and DAH produces significantly larger micelles. These observations are consistent with incorporation of both resorcinol and DAH into F127 micelles. Experiment 5 (Table 3) is



Table 3 Particle sizes measured in DLS for the solution of the reaction steps

Expt	Composition	Particle size (nm)
1	$F127 + H_2O/EtOH$	1.17
2	$F127 + H_2O/EtOH+DAH$	1.15
3	F127 + Resorcinol +H ₂ O/EtOH	3.25
4	F127 + Resorcinol +DAH + H ₂ O/EtOH	5.91
5	$F127 + Resorcinol + DAH + H_2O/EtOH + H_2O$	20.67 ^a
6	F127 + Resorcinol +DAH + H ₂ O/EtOH +DMSO (for 1%metal complex)	1.76
7	F127 + Resorcinol +DAH + H ₂ O/EtOH +DMSO + 1%NiCsalen	538
8	F127 + Resorcinol +DAH + H ₂ O/EtOH +DMSO (for 5%metal complex)	2.01
9	F127 + Resorcinol +DAH + H ₂ O/EtOH +DMSO + 5%NiCsalen	616

^aThis sample separated into two phases, DLS was carried out on the upper phase

then particularly revealing. In this experiment the amount of water present in the added formalin produces spinodal decomposition and separation into two phases. However, the lower surfactant/resorcinol rich phase when cured by heating did not give a solid. When the two-phase reaction mixture was left overnight with stirring it gave a sticky, pale yellow paste which suggests that even in the absence of formaldehyde some type of polymerization reaction occurs. These experiments, therefore, suggest that the spinodal decomposition is produced, not by the insolubility of the growing polymer, but perhaps rather by the solution becoming so water rich that the F127/resorcinol/DAH micelle phase is no longer sufficiently soluble, and the system separates into two phases. The polymerization reaction freezes this phase separation process before the solution can separate into two layers. It could be argued that the presence of the formaldehyde in the added formalin would make the solution somewhat less water rich, and so less prone to undergo phase separation. However, even if this was the case, it is clear that the reaction mixture is close to a phase transition and so primed to undergo spinodal decomposition as polymerization proceeds.

Experiments 6–9 in Table 3 address the impact of addition of the salen complex. The salen complex has limited solubility in the water/ethanol mixture used as solvent and is dissolved in DMSO. Both the DMSO and the complex can potentially impact the properties of the polymer and resulting carbon. Comparing experiments 6 and 8 with experiment 4 shows that the effect of just DMSO is to decrease the size of the micelles. Addition of the salen complex results in loss of micelles, with formation of larger particles with diameters of ca. 500–600 nm. Presumably the

lack of solubility of the C-salen complex produces particles which the F127 binds to.

The nitrogen adsorption results are consistent with some fraction of the F127/DAH/resorcinol remaining bound to the C-salen particles. For the addition of 1 wt% nickel Csalen there is a significant drop in mesopore volume from the ca. 0.48 cm³/g for carbon heated to 500 °C without any additions [32], similar to the 0.157 cm³/g value observed for the nickel E-salen and higher than the 0.077 cm³/g value for the D-salen complex investigated previously [35]. Addition of 5 wt% nickel C-salen produces a much larger drop in mesopore volume: to 0.06 cm³/g, which is certainly consistent with more of the F127/DAH/resorcinol being bound to the C-salen particles resulting in less being available to drive self-assembly. The mesopore volumes for carbon heated to 800 °C are also interesting. In our earlier work on addition of 1 wt% E- and D-salen complexes, heating to 800 °C caused a collapse of the mesopores with barely measurable mesopore and micropore volumes (ca. 0-0.004 cm³/g). Here heating to 800 °C causes a drop in mesopore volume, but not the order of magnitude decline seen previously. The micropore volumes show similar behavior: addition of C-salen does not give the pronounced difference in behavior at 500 and 800 °C seen for the D and E-salens. This would appear to reflect the differences in structure of the three salen ligands. It was previously observed that the E-salen complexes gave higher mesopore values for a given metal than did the D-salen complexes: Csalen gives values more similar to the E-Salen than the Dsalen. The C-salen would be expected to be more thermally stable than the D-salen since there would less steric strain in the 6-membered ring. There are also two C-C bonds that would need to be broken to separate the two halves of the complex during pyrolysis which would lead to less disruption of the polymer and less collapse of the mesopores. But other factors, e.g., differences in solubility in the solvent and/or in the polymer as it is forming could also be involved.

Consideration of the SEM results gives further insight into the structure of the material, particularly on how the nickel is incorporated/dispersed over and in the carbon. Figures 3b and 4c show clearly the presence of clusters of nickel particles on the carbon surface (Fig. 3b) and buried within the carbon ligament (Fig. 4c). This is certainly consistent with the DLS results which show that the addition of the nickel C-salen complex leads to disappearance of the micelles and formation of larger particles. However, the EDS data, which shows small amounts of nickel everywhere in the monolith, the observation that the macropore structure is little altered by addition of the C-salen complex, and that a large mesopore volume is measured for the 1 wt% nickel sample, all argue that there must also be a considerable dispersion of the complex throughout the carbon.



Fig. 8 a Typical UV-vis spectra and b Compilation of concentration vs time for 1% NiCsalC500, 1%NiCsalC800, 5%NiCsalC500 and 5% NiCsalC800. Reaction conditions: 25 mL of 0.2 mol/L of NaBH₄, 50 mL of 0.0001 mol/L of PNP, weight of catalyst: 20 mg, ratio of NaBH₄ to PNP = 400:1

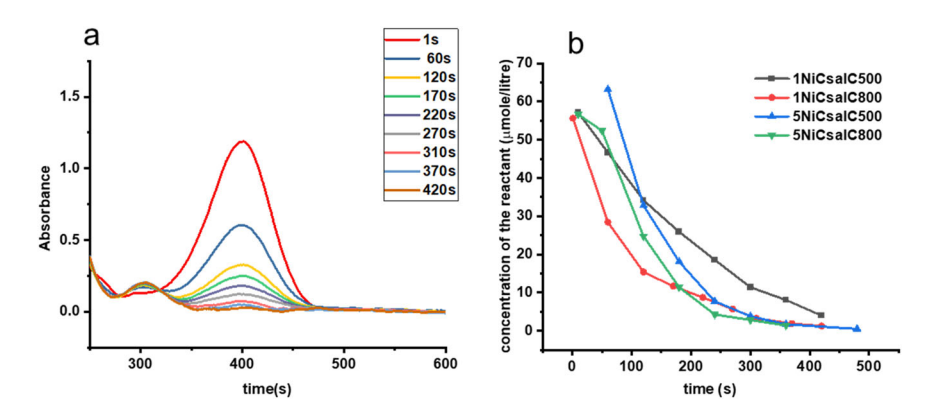


Table 4 Rates for heterogeneous catalysis

Sample	Rate constant $(s^{-1})^a$	Rate constant/gram Ni (s ⁻¹)
PNP, NaBH ₄ , no catalyst	$0.97 \pm 0.03 \times 10^{-3}$	$0.97 \pm 0.03 \times 10^{-3}$
1%NiCsalC500	$6.2 \pm 0.9 \times 10^{-3}$	31 ± 4.5
1%NiCsalC800	$8.7 \pm 0.7 \times 10^{-3}$	43 ± 3.5
5%NicsalC500	$12 \pm 1 \times 10^{-3}$	12 ± 1
5%NiCsalC800	$11\pm1\times10^{-3}$	11 ± 1

^aErrors are 95% confidence limits

That is, as the polymerization proceeds some of the initially large particles of nickel C-salen complex are dissolved into the polymer. A crude calculation shows that a 500 nm nickel C-salen particle could produce a single nickel nanoparticle with a diameter of ca. 25 nm. So, the clusters of particles observed in Fig. 2, c (which have particles sizes of up to ca. 30 nm) would appear to stem from larger nickel C-salen particles. It is possible that a smaller initial nickel C-salen particle could have given rise to a mixture of smaller nickel nanoparticles which then grew by diffusion of nickel atoms or smaller nickel nanoparticles produced elsewhere in the carbon and their incorporation into the larger nickel nanoparticles. In our previous work on two other types of metal salen complexes, considerable growth in metal nanoparticle size was observed when the pyrolysis temperature was increased from 500 to 800 °C. For the nickel C-salen complexes there are only small changes in the SEM particle sizes and calculated surface area, and modest increases in crystallite size. This generally matches the observed catalysis rates (Table 4) in which only small differences in rate are observed between the catalysts prepared at 500 °C and the equivalent catalysts prepared at 800 °C.

This is significantly different to what was observed for the E and D-salen complexes where dramatic growth of metal particles was observed between 500 and 800 °C. However, care needs to be exercised to avoid overinterpreting these results. SEM sees particles on the macropore walls; particles located within the carbon are not visible and so are not well sampled. Liquid phase catalysis similarly will be predominantly from the macropores, since the mesopores are so small that mass transport in and out of the mesopores will be limited. Despite these caveats it does appear that the C-salen gives smaller nickel particles which are less prone to growth at higher temperature than that seen for the E and D-salen complexes. Particle growth is likely to be a second-order process, i.e., higher local concentrations will give faster growth. Higher dispersion of the C-salen and higher thermal stability would both lead to slower particle growth. Beyond this, nickel nanoparticles formed within the carbon could move within the amorphous carbon. If the amorphous carbon does not wet the nickel then energy minimization would drive the nickel nanoparticles towards the mesopore and macropore walls. At higher temperatures the nickel nanoparticles can solubilize carbon leading to graphitization, the solubilization implies wetting of the nickel surface by the carbon, while the graphitic carbon does not wet nickel well. Depending upon the balance of these different factors it is possible to envisage conditions where there is a net movement of small nickel nanoparticles from within the carbon to the macropore wall surface which would result in the average nickel particle size remaining small.

The difference in rate between the 1 wt% nickel catalyst made at 500 °C and the 5 wt% nickel catalysts made at the same temperature is about what would be expected based on the calculated surface area: the 1 wt% has about twice the surface area per gram of the 5 wt% sample, so 5 wt% nickel would be expected to have ca. 2.5 times the total surface area. For the samples heated to 800 °C, the difference in surface area/gram is similar, but the increase is rate constant is only about 25%.

Preliminary studies were carried out to determine the recyclability of the catalyst. The results are given in Table S4 in the supplementary information and show that the rate of conversion drops to about 50% in the 5th cycle of use. In a batch experiment loss of activity is likely to be the result of agglomeration of the nanoparticles, leading to loss of



surface area. For use in a fixed bed reactor it is not clear how meaningful this result would be. For these batch experiments the carbon was ground finely to enable the catalysis experiments to be carried out, such grinding could dislodge particles and so make them more mobile. Against this, in a fixed bed reactor there is a net flow of fluids through the catalyst that will tend to exacerbate any leaching of the metal by a liquid reagent or a solvent. Liquids will also tend to apply more force to metal nanoparticles which may well be dislodged and so washed out of a fixed bed. In previous work on hierarchically porous silica supporting silver nanoparticles we have seen evidence of both of these mechanisms occurring [41]. In gas phase reactions that are commonly carried out using fixed beds the force imparted by the moving fluid is expected to be significantly lower and there would not be expected to be dissolution of catalyst into a liquid phase. The likely modes of catalyst deactivation are therefore expected to be significantly different from those in a liquid phase batch study.

In our previous work we found that there was a significant difference in the size of metal nanoparticles/ nanostructures observed in going from the D-salen metal complexes where the two halves of the salen ligand were bridged by the linear 6 carbon bridge and the E-salen metal complexes where the two halves were bridged by a 2carbon bridge. The cyclohexyl bridge of the C-salen ligand appears to confer a further improvement in metal nanoparticle size. We do not think this improvement is the result of differences in solubility of the salen complexes. All three complexes required addition of DMSO to disperse them. The observation of clusters of nanoparticles for C-salen rather than the observation of large isolated metal nanostructures such as seen for the D-salen implies that clumps of complex within the polymer is not sufficient, by itself, to give growth of large metal nanostructures such as seen for the D-salen. Instead, it seems more likely that all three complexes formed large (>500 nm) sized particles of complex, which for the D-salen in particular seeds growth of large metal nanostructures during the carbonization process. It is unclear whether the differences in metal nanoparticle size result from stronger binding of the metal ion to the ligand, or if the ligand itself is more thermally stable so that the two halves of the ligand remain bound to the metal ion to a higher temperature. These are scarcely the only possibilities, but our observation that even relatively minor changes in the structure of the ligand can impact the size of the resulting nanoparticles suggests that further optimization of such complexes can further improve the size and dispersion of the nanoparticles. In particular, from this work improvements of the solubility of the complex would be expected to substantially improve the dispersion of the complex within the polymer and so is predicted to improve the metal nanoparticle dispersion.

5 Conclusions

The limited solubility of the nickel C-salen complex in the water/ethanol mixture used in this study has an adverse impact on the extent of mesopore formation and nickel nanoparticle dispersion. DLS results suggest that this occurs because the complex forms 500-600 nm sized particles in solution and that such particles bind significant amounts of the surfactant making them less available for forming mesopores. The poor dispersion of the complex in solution then likely results in incomplete dispersion of the complex in the polymer. In the final carbon the poor dispersion leads to clumps of nickel nanoparticles both on the surface and incorporated into the body of the carbon. The nickel particle size is sufficiently small for carbon made with the nickel C-salen that the material functions as a catalyst for the reduction of nitrophenol by sodium borohydride in water.

Acknowledgements The use of instruments in the Central Analytical Facility at The University of Alabama is acknowledged as is the required cost match from the Bakker Research Gift Fund. TVK acknowledges support from the Research Simulation program of the Office of Research at The University of Alabama, and RA acknowledges support from a Palmer Scholarship.

Compliance with ethical standards

Conflict of interest The University of Alabama has been issued a patent that covers work in this paper. Under University of Alabama policies MGB, KHS, and TVK, as the inventors of this patent, would gain monetarily from licensing of the patent.

Publisher's note Springer Nature remains neutral with regard to jurisdictional claims in published maps and institutional affiliations.

References

- Auer E, Freund A, Pietsch J, Tacke T (1998) Appl Catal A 173:259–271
- Menéndez-Díaz JA (2006) Martín-Gullón I Types of carbon adsorbents and their production, in: TJ Bandosz (Ed.) Activated carbon surfaces in environmental remediation, Elsevier, New York, pp. 1–47
- Neimark AV, Kheifez LI, Fenelonov VB (1981) Ind Eng Chem Prod Res Dev 20:439–450
- 4. Pekala RW (1989) J Mater Sci 24:3221-3227
- Pekala RW, Alviso CT, Kong FM, Hulsey SS (1992) J Non-Cryst Solids 145:90–98
- Moreno-Castilla C, Maldonado-Hodar FJ (2005) Carbon 43:455–465
- Zapata-Benabithe Z, de Vicente J, Carrasco-Marin F, Moreno-Castilla C (2013) Carbon 53:399–413
- Perez-Cadenas AF, Ros CH, Morales-Torres S, Perez-Cadenas M, Kooyman PJ, Moreno-Castilla C, Kapteijn F (2013) Carbon 56:324–331
- Kim CHJ, Zhao D, Lee G, Liu J (2016) Adv Funct Mater 26:4976–4983
- Jia X, Dai B, Zhu Z, Wang J, Qiao W, Long D, Ling L (2016) Carbon 108:551–560



- Zhang X, Zhao J, He X, Li Q, Ao C, Xia T, Zhang W, Lu C, Deng Y (2018) Carbon 127:236–244
- Chuenchom L, Kraehnert R, Smarsly BM (2012) Soft Matter 8:10801–10812
- Lu A-H, Smått J-H, Lindén M (2005) Adv Func Mater 15:865–871
- Huang Y, Cai H, Feng D, Gu D, Deng Y, Tu B, Wang H, Webley PA, Zhao D (2008) Chem Commun 2641–2643
- Hua ZL, Gao JH, Bu WB, Zhang LX, Chen HR, Shi JL (2009) J Sol-Gel Sci Technol 50:22–27
- 16. Liang C, Dai S (2009) Chem Mater 21:2115-2124
- Hao G-P, Li W-C, Qian D, Lu A-H (2010) Adv Mater 22:853–857
- Hao G-P, Li W-C, Qian D, Wang G-H, Zhang W-P, Zhang T, Wang A-Q, Schuth F, Bongard H-J, Lu A-H (2011) J Am Chem Soc 133:11378–11388
- Fang B, Kim JH, Kim M-S, Yu J-S (2013) Acc Chem Res 46:1397–1406
- 20. Sevilla M, Fuertes AB (2013) Carbon 56:155-156
- 21. Liu Y (2014) J Porous Mater 21:1009-1014
- Liu Y, Lin B, Li D, Zhang X, Sun Y, Yang H (2014) J Appl Polym Sci 132:41322. (41321 of 41327)
- 23. Tomasic V, Jovic F (2006) Appl Catal A 311:112-121
- Bénard S, Giroir-Fendler A, Vernoux P, Guilhaume N, Fiaty K (2010) Catal Today 156:301–305
- Tanimu A, Jaenicke S, Alhooshani K (2017) Chem Eng J 327:792–821
- Maresz K, Ciemiega A, Mrowiec-Białon J (2018) Catalysts 8 221:221–228

- Sachse A, Hulea V, Finiels A, Coq B, Fajula F, Galarneau A (2012) J Catal 287:62–67
- Fletcher PDI, Haswell SJ, He P, Kelly SM, Mansfield A (2011) J Porous Mater 18:501–508
- Pelisson C-H, Nakanishi T, Zhu Y, Morisato K, Kamei T, Maeno A, Kaji H, Muroyama S, Tafu M, Kanamori K, Shimada T, Nakanishi K (2017) ACS Appl Mater Interfaces 9:406–412
- Zhu Y, Kanamori K, Brun N, Pélisson C-H, Moitra N, Fajula FO, Hulea V, Galarneau A, Takeda K, Nakanishi K (2016) Catal Comm 87:112–115
- 31. Song W, Shi D, Tao S, Li Z, Wang Y, Yu Y, Qiu J, Ji M, Wang X (2016) J Colloid Interface Sci 481:100–106
- Kotbagi TV, Hakat Y, Bakker MG (2015) MRS Commun 5:51–56
- Kotbagi TV, Hakat Y, Bakker MG (2016) Mater Res Bull 73:204–210
- Kotbagi TV, Gurav HR, Nagpure AS, Chilukuri SV, Bakker MG (2016) RSC Adv 6:67662–67668
- Kotbagi TV, Shaughnessy KH, LeDoux C, Cho H, Tay-Agbozo S, van Zee J, Bakker MG (2017) J Sol-Gel Sci Techn 84:258–273
- Eshtiagh-Hosseini H, Beyramabadi SA, Mirzaei M, Morsali A, Salimi AR, Naseri MA (2013) J Struct Chem 54:1063–1069
- 37. Ding Y-Q, Cui Y-Z, Li T-D (2015) J Phys Chem A 119:4252–4260
- 38. Burke WJ (1949) J Am Chem Soc 71:609-612
- Ghosh NN, Kiskan B, Yagci Y (2007) Prog Polym Sci 32:1344–1391
- 40. Payne EW (1992) J Chem Ed 69:A40-A41
- 41. Hakat Y, Kotbagi TV, Bakker MG (2015) Processes 3:98-112

